

Controlling Surface Functionality through Generation of Thiol Groups in a Self-Assembled Monolayer

Simon Q. Lud,[†] Stefan Neppel,[‡] Gerhard Richter,[§] Paola Bruno,^{||} Dieter M. Gruen,^{||}
Rainer Jordan,^{§,⊥} Peter Feulner,[‡] Martin Stutzmann,[†] and Jose A. Garrido^{*,†}[†]Walter Schottky Institut, [‡]Physics Department E20, and [§]Wacker-Lehrstuhl für Makromolekulare Chemie, Department Chemie, Technische Universität München, 85747 Garching, Germany, ^{||}Materials Science Department, Argonne National Laboratory, Argonne, Illinois 60439, USA, and [⊥]Professur für Makromolekulare Chemie, Department Chemie, TU Dresden, 01069 Dresden, Germany

Received June 2, 2010. Revised Manuscript Received August 31, 2010

A lithographic method to generate reactive thiol groups on functionalized synthetic diamond for biosensor and molecular electronic applications is developed. We demonstrate that ultrananocrystalline diamond (UNCD) thin films covalently functionalized with surface-generated thiol groups allow controlled thiol–disulfide exchange surface hybridization processes. The generation of the thiol functional head groups was obtained by irradiating phenylsulfonic acid (PSA) monolayers on UNCD surfaces. The conversion of the functional headgroup of the self-assembled monolayer was verified by using X-ray photoelectron spectroscopy (XPS), near-edge X-ray absorption fine structure (NEXAFS), and fluorescence microscopy. Our findings indicate the selective generation of reactive thiol surface groups. Furthermore, we demonstrate the grafting of yeast cytochrome c to the thiol-modified diamond surface and the electron transfer between protein and electrode.

1. Introduction

A concept in surface patterning is focused on highly selective and addressable surface group generation that proceeds with high efficiency and in a one-step process. Surface modification of self-assembled monolayers (SAMs) by means of X-ray and electron irradiation has been the subject of numerous studies in the past years,^{1–6} since they may find applications in biosensing,⁷ organic solar cells,^{8,9} and molecular electronics.^{10–12} In particular, aromatic self-assembled monolayers have been successfully employed for the generation of chemical patterns via the selective conversion of nitro head groups into amino groups using low-energy electrons as well as X-ray irradiation.^{1–5} These currently existing approaches for the generation of amino head groups mainly aim at subsequent peptide bond formation, but also to

other coupling strategies,^{13,14} which require harsh chemistry and often involve difficulties in finding optimal coupling conditions for immobilization of nanoparticles or biomolecules. Here, we follow a novel approach, making use of molecular binding that can be achieved by free-standing reactive sulfhydryl groups. For this purpose, we have developed a procedure which enables the preparation of thiol-terminated aromatic SAMs covalently grafted to ultrananocrystalline diamond (UNCD) surfaces. Diamond thin films have received much attention for biosensing applications^{15–17} due to a unique combination of material properties such as good biocompatibility,¹⁸ high chemical stability in aqueous environment, excellent electrochemical performance,¹⁹ and the ability to form stable covalent bonds with organic molecules and biomolecules.¹⁵ In particular, UNCD films²⁰ were shown to outperform other materials such as quartz, Au, or silicon for DNA immobilization.¹⁵ Furthermore, the superior electrochemical properties of diamond thin films as electrodes were shown to be suitable for the development of enzyme-modified diamond biosensors.¹⁶ Thus, UNCD surfaces have been employed in this work because of their potential in the field of biosensors. We have demonstrated the selective generation of thiol groups by X-ray- and electron-induced modification of monophenyl monolayers covalently grafted to diamond surfaces

*Corresponding author. Jose A. Garrido. Phone: ++49-89 289 12766. E-mail: garrido@wsi.tum.de.

(1) Götzhäuser, A.; Eck, W.; Geyer, W.; Stadler, V.; Weimann, T.; Hinze, P.; Grunze, M. *Adv. Mater.* **2001**, *13*, 803–806.

(2) Götzhäuser, A.; Geyer, W.; Stadler, V.; Eck, W.; Grunze, M.; Edinger, K.; Weimann, T.; Hinze, P. *J. Vac. Sci. Technol., B* **2000**, *18*, 3414–3418.

(3) Geyer, W.; Stadler, V.; Eck, W.; Gölzhauser, A.; Grunze, M.; Sauer, M.; Weimann, T.; Hinze, P. *J. Vac. Sci. Technol., B* **2001**, *19*, 2732–2735.

(4) Geyer, W.; Stadler, V.; Eck, W.; Zharnikov, M.; Gölzhauser, A.; Grunze, M. *Appl. Phys. Lett.* **1999**, *75*, 2401–2403.

(5) Eck, W.; Stadler, V.; Geyer, W.; Zharnikov, M.; Gölzhauser, A.; Grunze, M. *Adv. Mater.* **2000**, *12*, 805–808.

(6) Zharnikov, M.; Grunze, M. *J. Vac. Sci. Technol., B* **2002**, *20*, 1793–1807.

(7) Biebricher, A.; Paul, A.; Tinnefeld, P.; Götzhäuser, A.; Sauer, M. *J. Biotechnol.* **2004**, *112*, 97–107.

(8) Senadeera, G. K. R.; Kitamura, T.; Wada, Y.; Yanagida, S. *J. Photochem. Photobiol., A* **2004**, *164*, 61–66.

(9) Campoy-Quiles, M.; Ferenczi, T.; Agostinelli, T.; Etchegoin, P. G.; Kim, Y.; Anthopoulos, T. D.; Stavrinou, P. N.; Bradley, D. D. C.; Nelson, J. *Nat. Mater.* **2008**, *7*, 158–164.

(10) Elbing, M.; Blaszczyk, A.; von Haenisch, C.; Mayor, M.; Ferri, V.; Grave, C.; Rampi, M. A.; Pace, G.; Samori, P.; Shaporenko, A.; Zharnikov, M. *Adv. Funct. Mater.* **2008**, *18*, 2972–2983.

(11) Ferri, V.; Elbing, M.; Pace, G.; Dickey, M. D.; Zharnikov, M.; Samori, P.; Mayor, M.; Rampi, M. A. *Angew. Chem., Int. Ed.* **2008**, *47*, 3407–3409.

(12) Tai, Y.; Shaporenko, A.; Noda, H.; Grunze, M.; Zharnikov, M. *Adv. Mater.* **2005**, *17*, 1745–1742.

(13) Al-Rawashdeh, N. A. F.; Azzam, W.; Wöll, C. *Z. Phys. Chem. Int.* **2008**, *222*, 965–978.

(14) Schilp, S.; Ballav, N.; Zharnikov, M. *Angew. Chem., Int. Ed.* **2008**, *47*, 6786–6789.

(15) Yang, W. S.; Auciello, O.; Butler, J. E.; Cai, W.; Carlisle, J. A.; Gerbi, J.; Gruen, D. M.; Knickerbocker, T.; Lasseter, T. L.; Russell, J. N.; Smith, L. M.; Hamers, R. *J. Nat. Mater.* **2002**, *1*, 253–257.

(16) Hartl, A.; Schmich, E.; Garrido, J. A.; Hernando, J.; Catharino, S. C. R.; Walter, S.; Feulner, P.; Kromka, A.; Steinmüller, D.; Stutzmann, M. *Nat. Mater.* **2004**, *3*, 736–742.

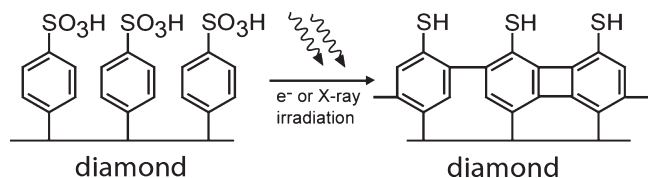
(17) Yang, N.; Uetsuka, H.; Osawa, E.; Nebel, C. E. *Angew. Chem., Int. Ed.* **2008**, *47*, 5183.

(18) Freitas, R. A., Jr. *Nanomedicine, Vol. IIA: Biocompatibility*; Landes Bioscience: Georgetown, TX, 2003.

(19) Swain, G. M.; Anderson, A. B.; Angus, J. C. *MRS Bull.* **1998**, *23*, 56.

(20) Gruen, D. M. *Annu. Rev. Mater. Sci.* **1999**, *29*, 211.

Scheme 1. X-ray- or Electron-Induced Conversion of the Functional Head Groups of the Aromatic Monolayer, Showing the Cross-Linked Molecules



(Scheme 1). To further prove the reactivity of the generated thiol groups, redox proteins were grafted to thiol-modified diamond electrodes, demonstrating the electron transfer between proteins and electrode. The novel surface group modification reported here addresses new strategies for chemical nanolithography, which can be used to create high-quality chemical patterns for further molecule or nanoparticle attachment.

2. Results and Discussion

In this study, phenylsulfonic acid (PSA) monolayers were prepared on hydrogen-terminated UNCD surfaces, as reported elsewhere.²¹ In short, the hydrogenated diamond surface was immersed into a saturated solution of 4-sulfobenzene diazonium tetrafluoroborate in 15 mL acetonitrile and stirred for 72 h. We have previously reported that highly dense phenyl monolayers can be obtained with this procedure.²¹ The PSA SAMs on diamond were irradiated with X-rays and electrons, resulting in significant changes of the corresponding XPS and NEXAFS spectra. More details on the experimental conditions can be found in the Experimental Section. During the irradiation, sets of elemental scans were successively recorded in selected energy regions. These spectra were then used to estimate the chemical conversion as a function of the X-ray or electron exposure.

Figure 1a shows the S2p high-resolution XPS signals with increasing X-ray dose for a functionalized PSA diamond surface. The topmost spectrum shows the structure of the pristine, unconverted SAM, followed by spectra recorded after progressive irradiation. During X-ray exposure with 265 eV light energy, we observed a partial loss of overall sulfur signal relative to the pristine sulfur and simultaneously the appearance of different sulfur species: A gradual conversion of the S2p_{3/2}/S2p_{1/2} doublet signal from 168.2 to 163.8 eV is clearly visible. The former binding energy²² is assigned to sulfur as in phenyl ring attached sulfonic acid groups, and its calculated peak area with respect to the C1s signal—data not shown—confirms the formation of approximately 80% of a dense monolayer, in good agreement with previous reports.²¹ The latter, increasingly dominant doublet corresponds to the chemical shift of a thiophenol S2p photoemission line, which has been observed at 163.2 eV.²³ The origin of the slight shoulder peak at 161.0 eV is tentatively attributed to the presence of atomic sulfur at the surface, resulting from the radiation-induced damage occurring in the aromatic monolayer. The intensities of the thiol S2p emission are displayed in Figure 1b, along with the total S2p intensity. The conversion and decay kinetics obey a first-order reaction and, thus, can be expressed by an exponential decay function (solid line), following

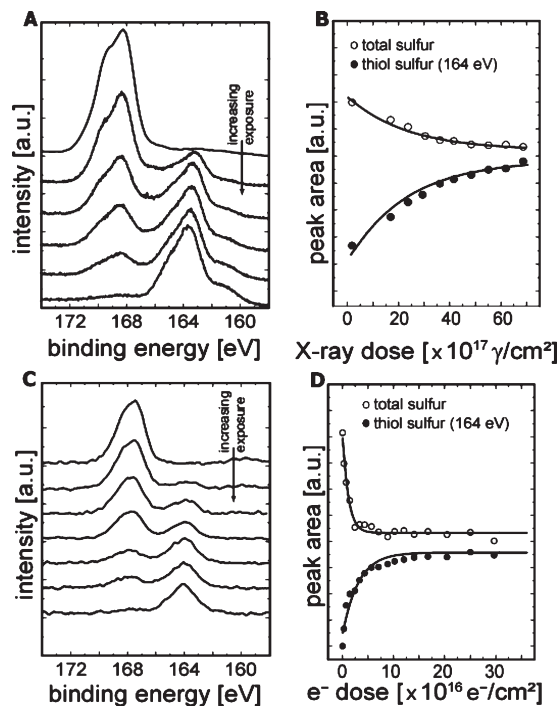


Figure 1. X-ray- and electron-induced conversion: Consecutive XP spectra of X-ray- (a) and electron- (c) irradiated PSA SAMs on diamond. Calculated dependence of signal fractions on exposure dose are shown in (b,d). The integral intensities of XPS features for all sulfur moieties (open circles), and the contribution exclusively related to thiol sulfur (full circles) derived from the XP spectra are fitted (—) using the first-order rate model of eq 1. Signal fractions are normalized to the total sulfur values for the corresponding pristine monolayer.

an analysis made by Olsen et al.²⁴ and modified later²⁵

$$I = I_{\text{SAT}} + (I_0 - I_{\text{SAT}}) \cdot \exp\left(\frac{-\sigma \cdot \Phi}{S}\right) \quad (1)$$

Here, I is the intensity value as a function of the cumulative particle exposure Φ , whereas I_0 and I_{SAT} are the intensity values for the pristine and completely irradiated monolayer, respectively. S is the area of the cumulative radiation exposure and σ the effective reaction cross-section parameter. Upon intense exposure to X-rays, an initially unexposed PSA monolayer shows about 21% loss in the S2p signal, with a corresponding loss cross section σ_L of $(3.7 \pm 0.6) \times 10^{-19} \text{ cm}^2$, resulting from fit analysis of the topmost curve in Figure 1b using eq 1. This loss is comparable to other observed losses for chemical lithography.²¹

The generation of surface thiol groups, on the other hand, has a conversion cross section value σ_C of $(7.5 \pm 0.9) \times 10^{-19} \text{ cm}^2$, as resulted from the fit of the lowermost line in Figure 1b to eq 1. Similar to the electron-induced reduction of the nitro groups observed by Eck et al.⁵ in monolayers of biphenyl molecules on Au, the conversion of surface sulfonic acid groups occurs in the absence of any external reducing or hydrogenating agents. The authors suggested that electron irradiation results in the cleavage of the C–H bonds, which is followed by cross-linking of the phenyl rings and hydrogenation of the nitro terminal groups.⁵ Each of the biphenyl molecules could provide the six hydrogen atoms required for a complete reduction of the nitro group. In our case, however, the SO₃H to SH conversion is assumed to be not a pure chemically driven reaction like a reduction with enthalpically favored redox-products, which would require more than the four

(21) Lud, S. Q.; Steenackers, M.; Jordan, R.; Bruno, P.; Gruen, D. M.; Feulner, P.; Garrido, J. A.; Stutzmann, M. *J. Am. Chem. Soc.* **2006**, *128*, 16884–16891.

(22) Nasef, M. M.; Saidi, H. *Appl. Surf. Sci.* **2006**, *252*, 3073–3084.

(23) Barriet, D.; Yam, C. M.; Shmakova, O. E.; Jamison, A. C.; Lee, T. R. *Langmuir* **2007**, *23*, 8866–8875.

(24) Olsen, C.; Rowntree, P. A. *J. Chem. Phys.* **1998**, *108*, 3750–3764.

(25) Zharnikov, M.; Frey, S.; Heister, K.; Grunze, M. *Langmuir* **2000**, *16*, 2697–2705.

hydrogen atoms each monophenyl molecule can provide. The conditions of the experiments—irradiation by high-energy electrons or photons—favor the case of highly excited, strongly antibonding molecular states. Thus, dissociation of fragments from the functional sulfonic group consisting of incompletely hydrogen-saturated oxygen compounds or even radicals are very likely.

Given the success of the X-ray-induced conversion, a successful electron-induced conversion is also expected, since the X-ray-induced conversion is expected to proceed not only by the primary photon-induced process, but also via secondary excitations through energetic photons and decaying electrons, as well as true secondary electrons.²⁶ Indeed, we observed X-ray irradiated spectra resembling electron beam irradiation spectra of SAM functionalized diamond surfaces. As shown by Figure 1c, qualitative changes appear in a series of S2p spectra acquired at increasing electron beam exposure. Compared to Figure 1a, nearly identical behavior of S2p_{3/2}/S2p_{1/2} doublet peaks regarding S2p binding energy shift and peak intensity decay is observed. The shoulder at 161 eV cannot be resolved in the spectra shown in Figure 1c, owing to the lower resolution in the experiment.

Figure 1d displays the signal fraction evolution at the S2p peak region for the thiol species, as well as the total contribution of sulfonic and thiol species as a function of electron beam exposure. The overall sulfur loss is specified by a loss cross section σ_L of $(3.9 \pm 0.6) \times 10^{-17} \text{ cm}^2$; for sulfonic to thiol conversion, a value σ_C of $(5.3 \pm 0.7) \times 10^{-17} \text{ cm}^2$ is obtained from the analysis of Figure 1d using eq 1. The total sulfur peak area (SO₃H and SH) decreases upon prolonged electron irradiation dose (approximately 37% after dose of $3.2 \times 10^{16} \text{ e}^-/\text{cm}^2$), which indicates an irradiation-induced partial loss of sulfur-containing molecular fragments. These values are comparable with those previously reported for the damage and modification of organic self-assembled monolayers on gold by low-energy electrons.²⁷

For the comparison of the electron and X-ray-induced conversions, one can use the characteristic dose after which 37% of the sulfonic acid groups are converted, which corresponds to about $350 \times 10^{16} \text{ 265 eV photons/cm}^2$ (nonresonant X-ray-induced conversion) and $3.2 \times 10^{16} \text{ electrons/cm}^2$ (electron-induced conversion). Accordingly, longer photon irradiation is needed to achieve the same quantity of sulfonic conversion than with electron irradiation, with a ratio of about 100:1. It is important to note that the ratio of the X-ray and electron attenuation lengths, which in a first approximation is proportional to the efficiency of the irradiation-induced conversion, depends to a large extent on the photon energy and to a lesser extent on the electron energy. It has been previously shown that the changes observed in response to nonresonant X-ray irradiation were nearly identical to those induced by electron irradiation, suggesting that the secondary electrons produced during X-ray irradiation are responsible for the resulting molecular changes.⁶ Larger photon-induced reaction rates are possible by tuning the photon energy to an outer or inner shell resonance. Resonant inner-shell excitations allow, in addition, allocating the energy at a distinct atom of the molecule with the result of selective bond modification (see ref 28 and references therein). However, the excessive costs for narrow bandwidth photons from synchrotron radiation sources ($\sim 3 \times 10^9$ US\$ for 1 mol of photons), the higher

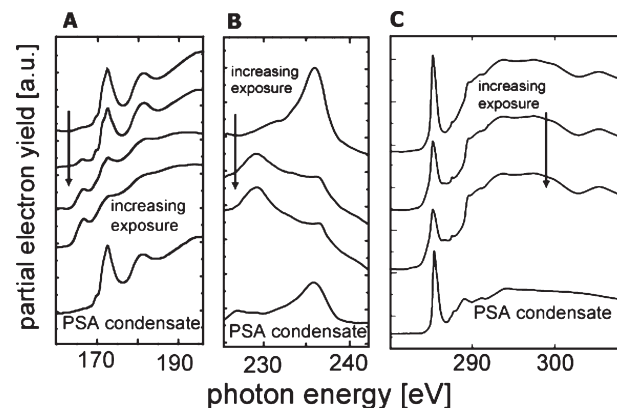


Figure 2. NEXAFS fingerprinting of the conversion process. Panels (a), (b), and (c) show the S2p, S2s, and C1s NEXAFS spectra of PSA SAMs on UNCD, respectively. Each of the panels shows the spectra of the pristine surfaces (topmost spectrum) and of surfaces upon consecutive irradiation with an X-ray dosage of 1.8 , 3.6 , and $4.8 \times 10^{18} \text{ } \gamma/\text{cm}^2$. The lowermost spectra in all graphs were obtained using differently prepared, nonirradiated multilayer condensates of PSA on a Si surface, and are shown for comparison. The irradiation induces the conversion of the sulfonic groups into thiol moieties. This conversion is revealed in (a) by the appearance of the S–H related σ^* resonance at 166.2 eV and the decrease of the S=O related π^* transition at 172.6 eV upon consecutive irradiation. Further details can be found in the text.

conversion efficiency induced by electron-irradiation, together with the increasing availability of electron beam sources (for instance, in electron microscopes) and the ability to focus electron beams to write patterns of only some nanometers suggest that nonresonant electron-induced irradiation is more versatile for the so-called chemical lithography.¹

In agreement with our findings based on XPS measurements, the NEXAFS spectra for the strongly X-ray irradiated PSA SAMs (Figure 2) show increasing thiol resonances for an increased irradiation dose. The lowest of all near-edge spectra represent the data for a molecular condensate of PSA, which was prepared on a gold-sputtered Si surface (see Experimental Section), showing excellent consistency with the pristine monolayer, and thus reflecting the ordered formation of the SAM. In Figure 2a, the S2p NEXAFS spectra of the pristine and progressively X-ray-irradiated SAMs are depicted. Upon exposure, a small σ^* resonance appears on the low-energy side, at 166.2 eV. Following the literature,²⁹ this resonance is characteristic for $\sigma^*(\text{S–H})$ transitions in sulfur moieties. The gradual peak enhancement indicates the formation of surface thiol groups on the irradiated film. Simultaneously, the $\pi^*(\text{S=O})$ transition located at 172.6 eV in the sulfur L-edge spectrum, which corresponds to sulfonic acid moieties,³⁰ decreases with higher X-ray dosage and, thus, further proves the successful headgroup conversion. Furthermore, and in accordance with the latter two findings, the peak at 181.1 eV, which is assigned to (S=O) transitions,³¹ progressively vanishes. The gradual decrease of both π^* resonances reflects the disappearance of the double-bonded sulfur oxygen compounds, while the increase of the σ^* resonance is associated with the generation of surface thiol groups on the monolayer. The variation of the S2s NEXAFS spectra (Figure 2b) upon exposure is comparable to

(26) Laibinis, P. E.; Graham, R. L.; Biebuyck, H. A.; Whitesides, G. M. *Science* **1991**, *254*, 981–983.

(27) Feulner, P.; Niedermayer, T.; Eberle, K.; Schneider, R.; Menzel, D.; Baumer, A.; Schimich, E.; Shaporenko, A.; Tai, Y.; Zharnikov, M. *Phys. Rev. Lett.* **2004**, *93*, 178302.

(28) Menzel, D.; Feulner, P. *J. Phys.: Condens. Matter* **2001**, *13*, 11249–11266.

(29) Jalilehvand, F. *Chem. Soc. Rev.* **2006**, *35*, 1256–1268.

(30) Sarret, G.; Connan, J.; Kasrai, M.; Bancroft, G. M.; Charrie-Duhaut, A.; Lemoine, S.; Adam, P.; Albrecht, P.; Eybert-Berard, L. *Geochim. Cosmochim. Acta* **1999**, *63*, 3767–3779.

(31) Sutherland, D. G. J.; Kasrai, M.; Bancroft, G. M.; Liu, Z. F.; Tan, K. H. *Phys. Rev. B* **1993**, *48*, 14989–15001.

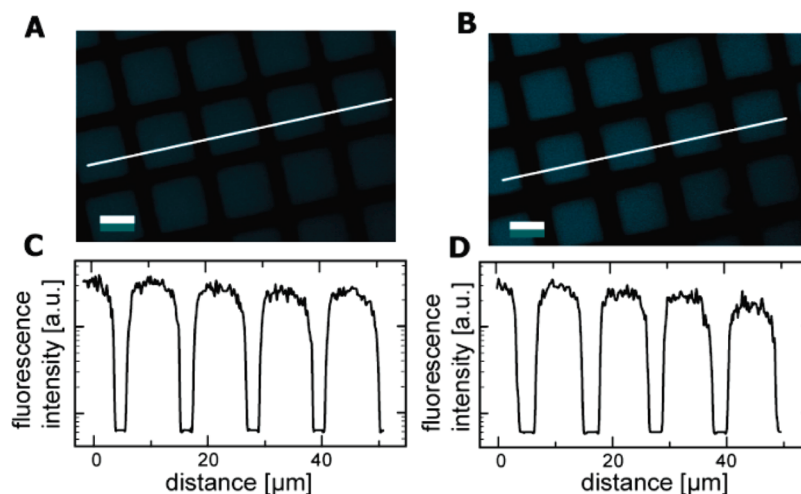


Figure 3. Fluorescence images of the (a) electron-beam-patterned and (b) X-ray-patterned PSA monolayers on diamond after reaction with the *N,N'*-didansyl-L-cysteine dye. (c,d) Cross sections along the white lines shown in (a) and (b), respectively. The dynamic range of fluorescence intensity corresponds to 2 orders of magnitude. The white scale bar represents 10 μm .

that of the S2p L-edge, the differences being attributed to the dependence of the resonance intensities on the dipole selection rule. X-ray exposure leads to a decrease of intensity of the $\pi^*(\text{S}=\text{O})$ NEXAFS resonances at 236.2 eV³² and an increase of the resonance intensity for the $\sigma^*(\text{S}-\text{H})$ peak located at 228.4 eV of thiol-containing molecules grafted to the diamond surface. The higher peak energies of the initial spectra indicate a higher sulfur oxidation state for the pristine layer, since reduced shielding of the nuclear charge increases the binding energies of the core orbitals. In Figure 2c, NEXAFS spectra at the C K-edge are depicted. These spectra show a decreasing $\text{C}1s \rightarrow \pi^*$ peak at 285.0 eV with increasing X-ray exposure, which we tentatively attribute to an irradiation-induced cross-linking process in the organic film. The X-ray-irradiated monolayer shows a drop of 60% in the characteristic absorption of the π^* peak, which is more than the surface coverage loss derived from the total intensity of the XPS S2p core level. We propose that the loss of the aromaticity in the layer, as a result of the cross-linking process, is the origin of the decaying π resonance. It is worth mentioning that molecular reorientation in the monolayer might also result in the observed π resonance variation. However, due to the random orientation expected from the UNCD substrate, we consider this effect to be negligible.

Fluorescence microscopy was performed on patterned molecular assemblies to further examine the chemical conversion, as well as the reactivity of the generated surface groups. The pattern of a metal mask was transferred to the monolayer on the diamond surface underneath, by electron irradiation or by a Mg $\text{K}\alpha$ X-ray source. In both cases, high doses were applied. Upon labeling with the fluorescence dye *N,N'*-didansyl-L-cysteine, via thiol–disulfide exchange, an intense fluorescence signal was only found on the electron or X-ray exposed surface squares, as depicted in Figure 3a and b. The unequal line-widths in the two images originate from the usage of a surface-clamped TEM plate as shadow mask. In addition, the fluorescence intensity on protected areas was close to the background level, as determined by photobleaching of a reference sample. As shown by the fluorescence intensity profile across several features of the surface in Figure 3c and d, the fluorescence intensity exhibits a contrast ratio of ~ 100 and reflects the high thiol density resulting from the surface modification.

Both images were recorded using identical fluorescence microscope settings.

Finally, the potential of this surface group modification in the fields of biosensors and bioelectronics is demonstrated by grafting a redox protein to thiol-modified diamond electrodes. Details of the protein grafting can be found in the Experimental Section. Yeast cytochrome c (YCC) has a unique surface cysteine residue, which makes this protein very attractive for oriented grafting.³³ The thiol-modified diamond electrodes were reacted with a highly concentrated YCC protein solution, to immobilize the protein through a thiol/disulfide exchange reaction.

Cyclic voltammograms (CVs) of (i) protein-modified and (ii) protein-free diamond electrode are shown in Figure 4. The presence of a pair of well-defined redox peaks in the protein-modified diamond electrode indicates the immobilization of YCC. These two peaks correspond to the $\text{Fe}^{2+}/\text{Fe}^{3+}$ transition of the YCC reaction center, and their position is in good agreement with previous results,³³ confirming that proteins are not denatured on the surface. From the analysis of the CVs experiments, we calculate a surface coverage of electroactive YCC of 12 ± 0.8 pmol/cm², which considering the theoretical dimensions of YCC ($3 \times 2.5 \times 3.5$ nm³) approximately corresponds to a 0.63 full-monolayer coverage. The presence of YCC has been further investigated using AFM. To this end, a PSA-modified UNCD substrate which was previously polished (see Experimental Section), was micropatterned by electron irradiation through a metal mask to generate the reactive surface sulfhydryl groups and then incubated in a highly concentrate YCC protein solution to immobilize the proteins. Figure 4b shows a tapping-mode AFM image recorded after the immobilization of the protein in liquid environment. The image indicates a dense surface coverage, and the section analysis of a line across the protein pattern (see Figure 4c) reveals the presence of a layer with an apparent height of about 3 nm, in good agreement with the dimensions of the protein.

3. Conclusions

In summary, we have demonstrated the X-ray- and electron-induced modification of surface sulfonic groups to thiol groups on monophenyl monolayers covalently grafted to diamond surfaces.

(32) Fraxedas, J.; Lee, Y. J.; Jimenez, I.; Gago, R.; Nieminen, R. M.; Ordejón, P.; Canadell, E. *Phys. Rev. B* **2003**, *68*, 195115.

(33) Heering, H. A.; Wiertz, F. G. M.; Dekker, C.; de Vries, S. *J. Am. Chem. Soc.* **2004**, *126*, 11103–11112.

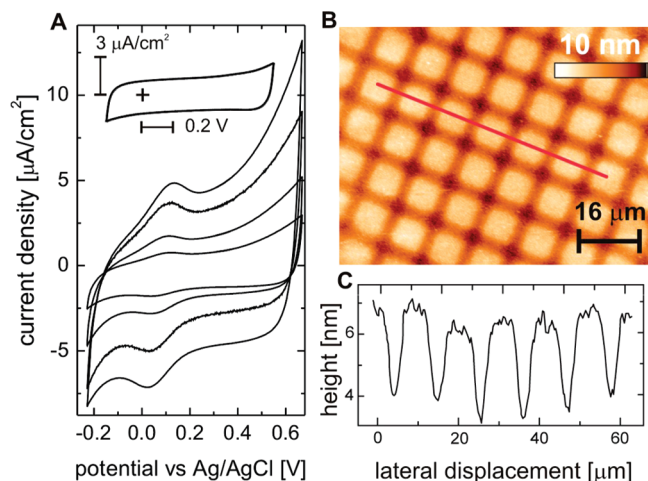


Figure 4. Yeast cytochrome c (YCC) proteins on diamond surfaces. (a) Cyclic voltammograms of the YCC-modified diamond electrode, measured in 10 mM KCl electrolyte buffered at pH 7. The scan rates corresponds to 50, 200, 300, and 400 mV/s. The potential axis is defined versus the silver/silver chloride electrode, and the inset shows the CV of a thiol-converted PSA-functionalized diamond electrode, where the cross indicates the zero values for electrode potential and current. The redox activity centered around +80 mV vs Ag/AgCl is attributed to the $\text{Fe}^{3+}/\text{Fe}^{2+}$ transition in the protein heme group. (b) Tapping-mode AFM height image ($80 \times 60 \mu\text{m}^2$, z -range 10 nm) of a polished ultrananocrystalline diamond surface in aqueous electrolyte after a patterned thiol-functionalization and covalent bonding of YCC (see Experimental Section). (c) Cross-section analysis of the line shown in (b), revealing a layer with a thickness of about 3 nm, in agreement with the protein height.

On the basis of the present results, we suggest that the sulfur moieties at the chain-termination groups are reduced, and that is accompanied by a cross-linking of the monolayer. The resulting thiol groups could be further chemically modified, providing a new route for surface immobilization of, for instance, biomolecules based on disulfide bridging. Following this approach, yeast cytochrome c proteins were grafted to thiol-modified diamond electrodes, which exhibit direct charge transfer between the immobilized proteins and the electrode surface. The irradiation-induced selective patterning presented here for diamond surfaces is expected to work with sulfonic-terminated aromatic self-assembled monolayers prepared on other substrates, provided the irradiation is homogeneous and the SAM layer is ordered and dense enough to facilitate the cross-linking; thus, only in the case of relatively flat surfaces is the irradiation-induced conversion expected to be efficient.

4. Experimental Section

Diamond Growth and Surface Preparation. All samples employed were about 1- μm -thick ultrananocrystalline diamond (UNCD) layers grown by microwave-assisted chemical vapor deposition on 600- μm -thick n-doped 100-oriented silicon substrates. Conductive UNCD films were obtained by using a $\text{N}_2/\text{Ar}/\text{CH}_4$ gas mixture (with 20% nitrogen content) as gas precursor.^{5,34} Typically, UNCD films have grains with a diameter between 5 and 10 nm and a surface roughness of about 10 nm rms. For the AFM experiments, the UNCD films were polished using a SF1 polishing fluid (Logitech Ltd., Glasgow), resulting in a surface rms below 1 nm on a regular basis.

Hydrogenation was performed in a vacuum chamber using a hydrogen gas flow of 300 sccm at a constant pressure of 1.5 mbar over a hot (2000 °C) tungsten filament, placed at a distance of 4 cm from the substrate. During the process, the sample temperature (approximately 700 °C) is monitored with a thermocouple.

Surface Functionalization. The hydrogenated diamond surface was immersed into saturated solution of 4-sulfobenzendiazonium tetrafluoroborate in 15 mL acetonitrile and stirred for 72 h. During the reaction, a gradual color change of the initially transparent reaction solution to a bright yellow and finally to a deep red color was observed. The PSA condensate was prepared by dropping a 10 M solution of PSA in pure ethanol on a gold-sputtered silicon wafer and dried with nitrogen.

N,N' -Didansyl-L-cysteine was used as a fluorescent dye and 0.5 mg/mL were dissolved in a 0.1 M Tris buffer solution at pH 8.5 and reacted with the patterned and functionalized diamond surface for 24 h at 4 °C in the dark.³⁵ Following the reaction, the surface was thoroughly rinsed with 0.1 M Tris buffer at pH 8.5 and sonicated in the same buffer solution for 30 min.

Immobilization of YCC. PSA-functionalized UNCD samples were modified by planar electron irradiation to generate the reactive sulphydryl surface groups and then incubated to a highly concentrated YCC protein solution to immobilize the protein through a thiol/disulfide exchange reaction. By the use of tris-(2-carboxyethyl)phosphine³⁶ as a reducing agent for the protein according to a traditional protocol, the substrate reaction was performed in a 0.1 M Tris buffer solution at pH 8.5 and reacted with the functionalized diamond surface for 24 h at 4 °C in the dark.

Irradiation Induced Conversion. X-ray irradiation was performed with synchrotron X-rays with an energy of 265 eV. Planar electron beam irradiation was performed by scanning the surface in a UHV system with an electron gun operating also at 300 eV together with a dedicated current integrator. A transmission electron microscopy grid (2000 mesh, Plano GmbH) was employed as a shadow mask to transfer a pattern to the monolayer-functionalized surface using electrons at the same voltage with a dose of 50 mC/cm².

X-ray Photoelectron Spectroscopy and Near-Edge X-ray Absorption Fine Structure. Photoelectron spectroscopy was carried out either in the synchrotron radiation facility BESSY-II (Berlin) at the undulator beamline U49/2-PGM1 with 265 and 390 eV light energy for the S2p and the C1s range, respectively, or using a Mg K_{α} X-ray laboratory source (1253.6 eV). The NEXAFS spectra have been recorded at the U49-II-PGM-1 beamline at BESSY, Berlin, and are normalized to the incident photon flux, which was measured using a photodiode.³⁷

The E vector of the synchrotron light was parallel to the surface normal for all NEXAFS measurements. We used a partial intensity analysis (PIA) for quantitative XPS. However, some corrections are necessary before XPS intensities from different elements can be mutually compared and quantified. The X-rays penetrate the material and excite photoelectrons. We used the inelastic mean free path (IMFP) to relate the ratio of the carbon substrate peak to the respective surface termination peak. Important is the number of atomic surface and subsurface layers contributing to the C1s signal: We convert the mass density of ultrananocrystalline diamond, $\rho = 3.3 \text{ g/cm}^3$, to an atomic density of $N_V = 1.6 \times 10^{23} \text{ cm}^{-3}$ and multiplied by the escape depth IMFP multiplied with a measuring geometry factor – product of the latter two denoted as l . Finally, we end with the number of carbon atoms per area contributing to the C1s XPS signal

$$N_{\text{C1s}} = l \cdot N_V = (1.7 \pm 0.3) \cdot 10^{16} \text{ cm}^{-2}$$

(34) Bhattacharyya, S.; Auciello, O.; Birrell, J.; Carlisle, J. A.; Curtiss, L. A.; Goyette, A. N.; Gruen, D. M.; Krauss, A. R.; Schlueter, J.; Sumant, A.; Zapol, P. *Appl. Phys. Lett.* **2001**, *79*, 1441–1443.

(35) Daly, T. J.; Olson, J. S.; Matthews, K. S. *Biochemistry* **1986**, *25*, 5468–74.

(36) Ruegg, U. T.; Rudinger, J. *Methods Enzymol.* **2007**, *47*, 111–116.

(37) Neppi, S.; Bauer, U.; Menzel, D.; Feulner, P.; Shaporenko, A.; Zharnikov, M.; Kao, P.; Allara, D. L. *Chem. Phys. Lett.* **2007**, *447*, 227–231.

This value has to be compared with surface atom densities, which typically reach $2 \times 10^{15} \text{ cm}^{-2}$ for the randomly oriented and reconstructed UNCD surfaces. Thus, we end up in around 7–10 atomic carbon layers contributing to the measured core level excitation signal.

Electrochemical Measurements. Cyclic voltammetry experiments were performed using a PARSTAT 2263 potentiostat (Princeton Applied Research). The three-electrode glass cell consisted of a Ag/AgCl reference electrode (MetroOhm AG, Germany) and a platinum wire counter electrode. Experiments were performed at room temperature in a 10 mM KCl buffer solution at pH 7. For determination of the protein surface coverage from the area under the voltammetric peaks, background curves of the protein-free electrode were subtracted.

From the area of the anodic and cathodic peaks, the total amount of charge passing through the electrode Q can be calculated. The surface coverage Γ can then be calculated using Faraday's law, $Q = nFA\Gamma$ where n is the number of

electrons involved in the $\text{Fe}^{3+}/\text{Fe}^{2+}$ redox reaction, A is the electrode area, F is Faraday's constant, and Γ is the average covered surface (mol/cm^2).

AFM Measurements. Atomic force microscopy measurements were performed at the solid/liquid interface in tapping mode with a Nanoscope IIIa system equipped with a fluid cell (Veeco Instruments, Santa Barbara, USA). Images were recorded in 0.1 M phosphate buffer (pH 7.0) at a scan speed of 500 nm/s and a resolution of 512×512 data points.

Acknowledgment. The project was funded by the DFG (project GA1432/1-1), the Nanosystems Initiative Munich (NIM), and the TUM International Graduate School of Science and Engineering (IGSSE). Work performed under the auspices of the U.S. Department of Energy (contract DE-AC02-06CH11357) at Argonne National Laboratory. S.N. and P.F. acknowledge support from the Helmholtz-Zentrum-Berlin and from the Munich Centre for Advanced Photonics via MAP C.1.5.